APPLICATION OF LATTICE BOLTZMANN METHOD IN PREDICTING FLOW OF SHEAR DRIVEN CAVITIES

Fudhail Abdul Munir[1], Nor Azwadi Che Sidik[2], Mohd Irwan Mohd Azmi[1] , Mohd Rody Mohamad Zin[1]

[1]Faculty of Mechanical Engineering, Universiti Teknikal Malaysia Melaka, Hang Tuah Jaya, 76100, Durian Tunggal, Melaka, MALAYSIA

[2]Universiti Teknologi Malaysia,86100,Skudai,Johor, MALAYSIA

Email: 1fudhail@utem.edu.my

ABSTRACT

In this paper, prediction of fluid flow in shear driven cavities is presented. Lattice Boltzmann Method is used as the alternative to conventional Computational Fluid Dynamics. The geometry of shear driven cavities as well as the Reynolds numbers is varied. The simulation is conducted for three types of shear driven cavities which are square cavity and triangular cavities. The obtained streamline patterns and the centre of vortex for each type is in excellent agreement with benchmark results. It is also found that the streamline patterns is significantly affected by the geometrical shape of cavities.

KEYWORDS: *Lattice Boltzmann Method, Computational Fluid Dynamics, shear driven cavites, streamline patterns.*

1.0 Introduction

Recently, due to rapidly increasing computational power, computational methods have become the essential tools to conduct researches in various engineering fields. In parallel to the development of high speed digital computer, computational fluid dynamics (CFD) has become the new third approach apart from theory and experiment in the philosophical study and development of the whole discipline of fluid dynamics (Anderson, 1995).

Solving the famous Navier-Stokes equation would require the knowledge of CFD since the non-linearity and complexity of the equation making it that there is currently no analytical solution to these equations except for a small number of special cases (Sidik, 2007). A few examples of numerical methods were introduced by experts in CFD field in order to solve the Navier-Stokes equation numerically. The methods are like Finite Difference Method, Finite Element Method and Finite Volume Method.

The Lattice Boltzmann Method (LBM) has become considerably alternative method to solve fluid flow (Munir et al , 2011). The way LBM works is by predicting the evolution of particle distribution function and calculates the macroscopic variables by taking moment to the distribution function.

The basic idea of Boltzmann work is that a gas is composed of interacting particles that can be explained by classical mechanics. The mechanics can be very simple where it contains streaming in space and billiard-like collisions interactions (Sidik, 2007). The starting point in LBM scheme is by tracking the evolution of the single-particle distribution. The concept of particle distribution has already well developed in the field of statistical mechanics while discussing the kinetics theory of gases and liquids. The definition implies that the probable number of molecules in a certain volume at certain time made from a huge number of particles in a system that travel freely, without collisions, for distances (mean free path) long compared to their sizes. Once the distribution functions are obtained, the hydrodynamics equation can be derived.

There are many advantages of LBM as compared to the conventional computational fluid dynamics. One of the main merits of LBM is that it has been proven successfully able to solve compressible Navier-Stokes equations (Malapinas et al., 2010). Apart from that, the algorithm of LBM can be easily re-worked to enable it to be applied on more complex simulation components (Mohd Irwan et al., 2010).

1.1 Mesoscale Lattice Boltzmann Model

Ludwig Boltzmann (1844-1906) introduced a transport equation based on statistical mechanics describing the evolution of gas particle in a system as;

$$\frac{\partial f}{\partial t}+c\ \frac{\partial f}{\partial x}+a\frac{\partial f}{\partial c}=\Omega \qquad (1)$$

where f, $\mathbf{c}$, $\mathbf{a}$ and c stand for density distribution function, mesoscopic speed, acceleration due to external force and collision function respectively. If there is no external force, Eq. (1) is no more than a hyperbolic wave equation with source term given as

$$\frac{\partial f}{\partial t}+c\ \frac{\partial f}{\partial x}=\Omega \qquad (2)$$

Any solution of the Boltzmann equation, Eq. (2), requires an expression for the collision operator . If the collision is to conserve mass, momentum and energy, it is required that

$$\int\begin{bmatrix}1\\ c\\ c^2\end{bmatrix}=\Omega dc=0 \qquad (3)$$

However, the expression for Ω is too complex to be solved. Even if we only consider two-body collision, the collision integral term needs to consider the scattering angle of the binary collision, the speed and direction before and after the collision, etc. Any replacement of collision must satisfy the conservation law as expressed in Eq. (3). The idea behind this replacement is that large amount of detail of two-body interaction is not likely to influence significantly the values of many experimental measured quantities (Succi, 2001).
There are a few version of collision operator published in the literature. However, the most well accepted version due to its simplicity and efficiency is the Bhatnagar Gross Crook

collision model with a single relaxation time (Bhatnagar et al., 1954). The equation that represents this model is given by ;

$$\Omega = -\frac{f - f^{eq}}{\tau} \tag{4}$$

where f^{eq} is the equilibrium distribution function and τ is the time to reach equilibrium condition during collision process and is often called the relaxation time. Eq. (4) also describes that $1/\tau$ of non-equilibrium distribution relaxes to equilibrium state within time τ on every collision process. Substituting Eq. (4) into Eq. (2) yield

$$\frac{\partial f}{\partial t} + c\frac{\partial f}{\partial x} = -\frac{f - f^{eq}}{\tau_f} \tag{5}$$

The equation (5) above is known as Boltzmann Bhatnagar- Gross-Krook(BGK) equation.
Eq. (5) describes two main processes at mesoscale level. The left hand side refers to the propagation of distribution function to the next node in the direction of its probable velocity, and the right hand side represents the collision of the particle distribution functions. In lattice Boltzmann formulation, magnitude of c is set up so that in each time step t, every distribution function propagates in a distance of lattice nodes spacing Δx. This will ensure that distribution function arrives exactly at the lattice nodes after Δt and collides simultaneously.
In order to apply Eq. (5) into the digital computer, the mesoscopic velocity space has to be discretised. This can be done by discretising the physical space into uniform lattice nodes. Every node in the network is then connected with its neighbours through a number of lattice velocities to be determined through the model chosen. The general form of the lattice velocity model is expressed as D_nQ_m where D represents spatial dimension and Q is the number of connection (lattice velocity) at every node. There are many lattice velocity models published in the literature, however, the most well used due to its simplicity is D2Q9.

1.2 The Lattice Boltzmann Equation Descretization

The Boltzmann equation with BGK collision model is as below:

$$\frac{\partial f}{\partial t} + c\frac{\partial f}{\partial x} = -\frac{f - f^{eq}}{\tau_f} \tag{5}$$

where Eq. (5) is well-known as the BGK Boltzmann equation as stated in previous sub section. The Maxwell-Boltzmann equilibrium distribution function is defined as (Liboff, 1990)

$$f^{eq} = \rho\left(\frac{1}{2\pi RT}\right)^{D/2} \exp\left\{-\frac{(\mathbf{c}-\mathbf{u})^2}{2RT}\right\} \tag{6}$$

The BGK lattice Boltzmann equation can be derived by further discretise Eq. (5) using an Euler time step in conjunction with an upwind spatial discretization and then setting the grid spacing divided by the time step equal to the velocity;

$$\frac{f(\mathbf{x},t+\Delta t)-f(\mathbf{x},t)}{\Delta t}+\mathbf{c}\frac{f(\mathbf{x}+\Delta\mathbf{x},t+\Delta t)-f(\mathbf{x},t+\Delta t)}{\Delta\mathbf{x}}=-\frac{f-f^{eq}}{\tau_f} \quad (7)$$

$$\frac{f(\mathbf{x},t+\Delta t)-f(\mathbf{x},t)}{\Delta t}+\mathbf{c}\frac{f(\mathbf{x}+\mathbf{c}\Delta t,t+\Delta t)-f(\mathbf{x},t+\Delta t)}{\mathbf{c}\Delta t}=-\frac{f-f^{eq}}{\tau_f} \quad (8)$$

As a result:

$$f(\mathbf{x}+\mathbf{c}\Delta t,t+\Delta t)-f(\mathbf{x},t)=-\Delta t\left(\frac{f-f^{eq}}{\tau_f}\right) \quad (9)$$

The equation above has a simple physical interpretation in which the collision term is evaluated locally and there is only one streaming step operation per lattice velocity. This stream and collide particle interpretation is a result of the fully Lagrangian character of the equation for which the lattice spacing is the distance traveled by the particles during a time step (Sterling, 1996).

Although first order discretizations have been used, the Lattice Boltzmann method is second order in both space and time when contributions that result from discretization error are taken to represent physics (Reider et al., 1995).

The macroscopic variables such as the density, ρ and flow velocity, $\mathbf{u}$ can be evaluated as the moment to the distribution function as follow

$$\sum f=\sum f^{eq}=\rho \text{ or } \int f d\mathbf{c}=\int f^{eq} d\mathbf{c}=\rho \quad (10)$$

$$\sum \mathbf{c}f=\sum \mathbf{c}f^{eq}=\rho\mathbf{u} \text{ or } \int \mathbf{c}f d\mathbf{c}=\int \mathbf{c}f^{eq} d\mathbf{c}=\rho\mathbf{u} \quad (11)$$

1.3 Prediction of flow for shear driven cavities by using LBM scheme

Over the years, fluid flow behaviors inside lid driven cavities have drawn many interested researchers and scientists. Examples of the applications of lid driven cavities are in material processing, dynamics of lakes, metal casting, galvanizing and etc. Two dimensional LBM simulation has been done successfully by Houat &Youcefi in 2011Numerous studies have been carried out on flow patterns inside a cavity. Excellent reviews on lid driven square cavity were done by (Ghia et al. , 1982), (Erturk et al., 2005) and (Erturk et al., 2007). Erturk et al. has successfully conducted simulation of flows inside triangular cavities. However, all these researchers conducted the fluid flow simulation by solving the Navier-Stokes equations.In addition to that, numerical simulations of fluid flow in square cavity by using LBM have been done by (Hou et al., 1995). However, the Reynolds number had been used is only up to 7000. Apart from the square cavity, simulations of triangular cavity up to 500 by using LBM has been shown successfully by (Duan et al., 2007).

2.0 Method of solution to solve flow in shear driven cavities

In this section, the details of methodology in simulating fluid flow inside shear driven cavities are presented.

2.1 Simulation of flow for shear driven square cavity

The lid driven cavity flow is a flow inside a cavity where the top wall slides to the right at a constant speed of U while the other three walls are made stationary. This type of flow has been used as a benchmark problem for many numerical methods due to its simple geometry but complicated flow behaviors. The geometry of the square cavity for this problem is shown in **FIGURE 1.**

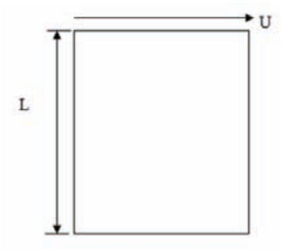

FIGURE 1 Geometry of shear driven square cavity

LBM is applied to this lid driven cavity flow of height L. The Reynolds number (Re) was varied from 100 to 10000. TABLE 1 shows the grid size used for the corresponding Reynolds numbers.

TABLE 1 Grid size for each Reynolds number for lid driven square cavity flow

Reynolds Number	Grid Size
100	400 x 400
400	400 x 400
1000	400 x 400
3200	400 x 400
5000	400 x 400
7500	400 x 400
1000	400 x 400

For triangular cavity case, three types of the triangular cavity geometry is selected for this problem. **FIGURE 2** shows the geometry of the triangles.

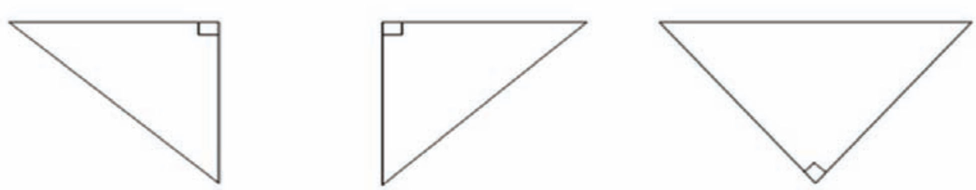

(a)Isosceles right triangle with 90 º at top right corner(type a)

(b)Isosceles right triangle with 90º at top left corner (type b)

(c)Isosceles right triangle with 90º at corner angle (type c)

FIGURE 2 Geometry of triangular cavities used

The grid size used for triangular cavity with 90° at top right corner is shown in **TABLE 2** below.

TABLE 2 Grid size for each Reynolds number for lid driven triangular cavity flow for triangular cavity' type a'

Reynolds Number	Grid Size
100	300 x 300
500	300 x 300
1000	300 x 300
1500	300 x 300
2000	300 x 300
2500	300 x 300

In addition to that, the grid size used for triangular type 'b'is shown in **TABLE 3** below.

TABLE 3 Grid size for each Reynolds number for lid driven triangular cavity flow for triangular cavity' type b'

Reynolds Number	*Grid Size*
100	*300 x 300*
500	*300 x 300*
1000	*300 x 300*
1500	*300 x 300*
2000	*300 x 300*
2500	*300 x 300*

TABLE 4 depicts the corresponding grid size with respect to Reynolds number.

TABLE 4 Grid size for each Reynolds number for lid driven triangular cavity flow for triangular cavity type ' c '

Reynolds Number	*Grid Size*
100	*400 x 200*
400	*400 x 200*
700	*400 x 200*
1000	*400 x 200*
3000	*400 x 200*
5000	*400 x 200*
7000	*400 x 200*
10000	*400 x 200*

For each case, velocity, U of 0.1 lu/s is applied on top side of the triangular cavities.
The simulation was done by using Fortran 90 language. The flowchart of the programming implementation is depicted in **FIGURE 3.**

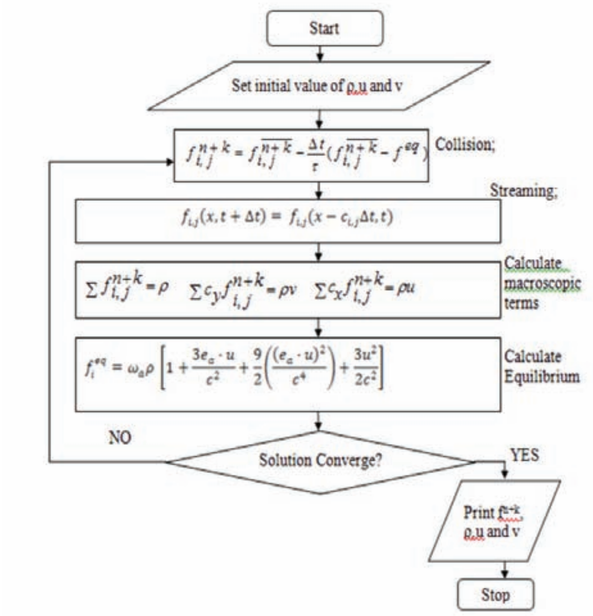

FIGURE 3 Flow chart of the execution of the programming

3.0 Simulation Results

3.1 Shear Driven Square Cavity

FIGURE 4 (a)-(h) shown below depicts the corresponding streamline contours for lid driven cavity square cavity.

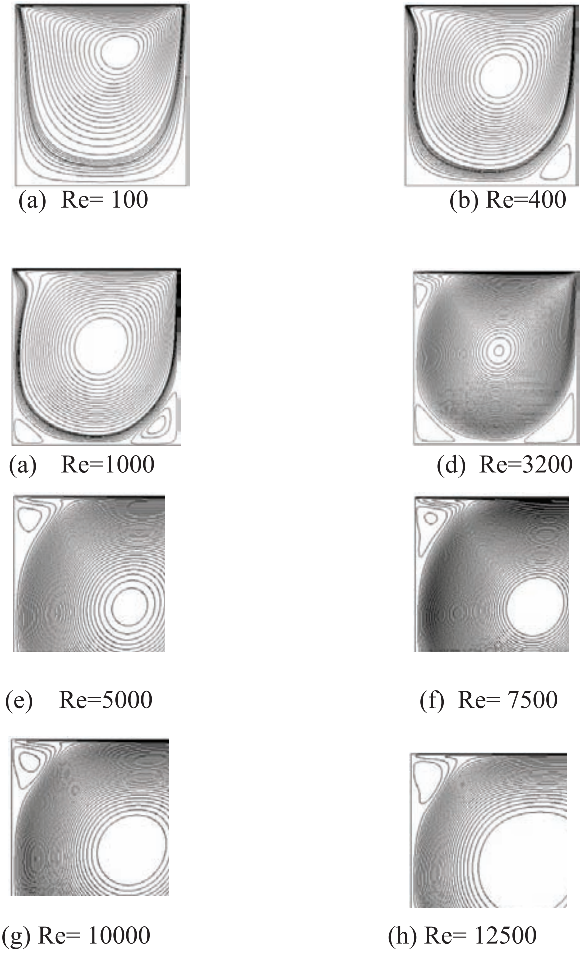

FIGURE 4 Streamline patterns for lid driven square cavity by using LBM scheme

From the **FIGURE 4** shown above, it can be deduced the number of secondary vortex increases when the Reynolds number is increased. For instance, when Reynolds number applied is 400, the first secondary vortex appears in the streamline patterns. The second secondary vortex appeared when Reynolds number is increased to 1000 as shown in **FIGURE 4** (b). The maximum number of secondary vortex appeared in the streamline contours for this type of problem is three.

Next, the location of the primary vortex for every Reynolds number was also calculated and is shown in **TABLE 5** below.

TABLE 5 Location of the centre of the primary vortex for lid driven square cavity.

Reynolds number (Re)	*Obtained Results*	*Reference benchmark (Ghia et al.,1982)*	*Reference Benchmark (Hou, et al., 1995)*
100	*(0.6200,0.7400)*	*(0.6172, 0.7344)*	*(0.6196,0.7373)*
400	*(0.5600,0.6000)*	*(0.5547,0.6055)*	*(0.5608,0.6078)*
1000	*(0.5300,0.5650)*	*(0.5313,0.5625)*	*(0.5333,0.5647)*
3200	*(0.5200, 0.5400)*	*(0.5165,0.5469)*	*NA*
5000	*(0.5150,0.5350)*	*(0.5117,0.5352)*	*(0.5176,0.5373)*
7500	*(0.5150,0.5235)*	*(0.5117,0.5322)*	*(0.5176,0.5333)*
10000	*(0.5133,0.5283)*	*(0.5117,0.5333)*	*NA*

From the results presented in **FIGURE 4** (a) to (h) and also TABLE 5, it is proven that the LBM is able to produce an excellent agreement with the results predicted by conventional numerical methods. They are apparent that the flow structures are in good agreement with the results published in the literature by previous researchers.

3.2 Isosceles triangular type 'a'

FIGURE 5 (a) to (f) show the streamline patterns of flow inside isosceles triangle cavity with 90° at top right corner.

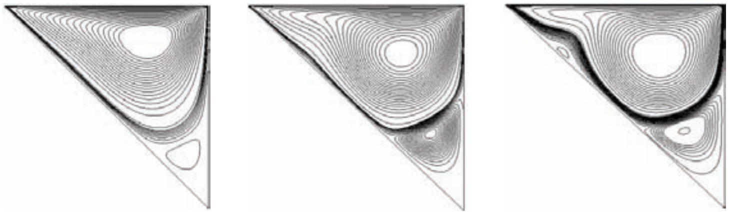

(a) Re=100 (b) Re=500 (c) Re=1000

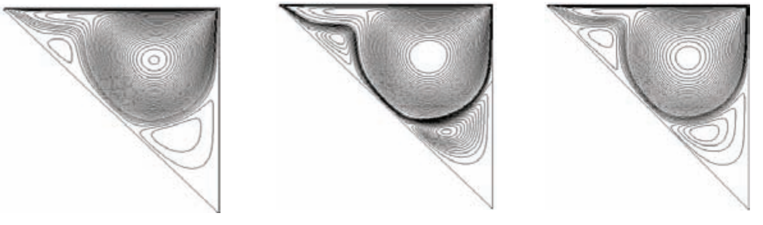

(d) Re=1500 (e) Re=2000 (e) Re=2500

FIGURE 5 Streamline patterns for isosceles triangular type 'a'

From the figures shown above, there are two significant features revealed by the streamline contours. The first feature is that the number of vortices is increased when the Reynolds (Re) numbers are increased. As we can see in **FIGURE 5** (c), the number of vortex is increased from previous which are two to three when the Re number is 1000. Furthermore, the second significant feature is that the centre of the primary vortex moves downstream to the right as Reynolds number is increased. For instance, **FIGURE 5**(a) depicts the centre of the primary vortex being located at 4/5 of the bottom vertex. However, this centre moves downward to 3/5 of the bottom vertex as the Reynolds number increases. Besides that, the primary vortex moves to downstream to the left as the value of the Reynolds number is increased. The location of the primary vortex for respective Reynolds number is shown in **FIGURE 6** below.

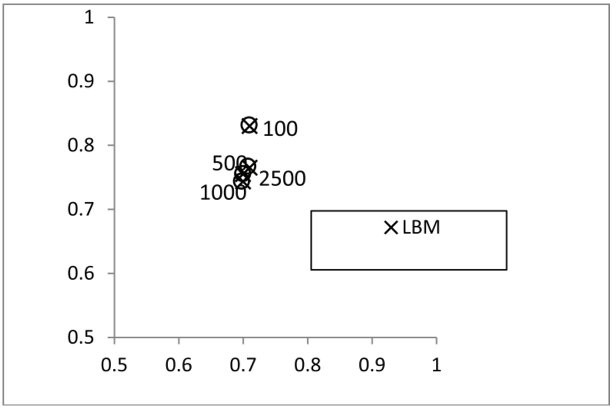

FIGURE 6 Effect of the Reynolds number to location of the centre of the primary vortex for isosceles triangular type 'a' is shown in figure below.

It is noticeable that the centre of the primary vortex moves downward to the left as the Reynolds number is increased. Apart from the plotted location of the primary vortex, the coordinate of the primary vortex is also compared with the existing benchmarks. The results is presented in TABLE 6 below.

TABLE 6 Location of the centre of the primary vortex for isosceles triangular type 'a'

Reynolds number	*Reference (Erturk & Gokcol ,2007)*	*Obtained Results by using LBM scheme*
100	*(0.7090,0.8320)*	*(0.7100,0.8300)*
500	*(0.7070,0.7676)*	*(0.7100,0.7650)*
1000	*(0.6992,0.7559)*	*(0.7000,0.7550)*
1500	*NA*	*(0.7000,0.7467)*
2000	*NA*	*(0.7000,0.7467)*
2500	*(0.6973,0.7441)*	*(0.7000,0.7433)*

From **TABLE 6** above, the results obtained is in good coherent as compared to the results done by previous researchers.

3.3 Isosceles triangular type 'b'

The results in term of streamline patterns for isosceles triangular type 'b' is shown in **FIGURE 7** (a)-(f) below. As shown in the figure, it is noticeable that the secondary vortex becomes bigger as Reynolds number increases. The second significant feature of the results obtained is the additional number of secondary vortex when Reynolds number is higher.

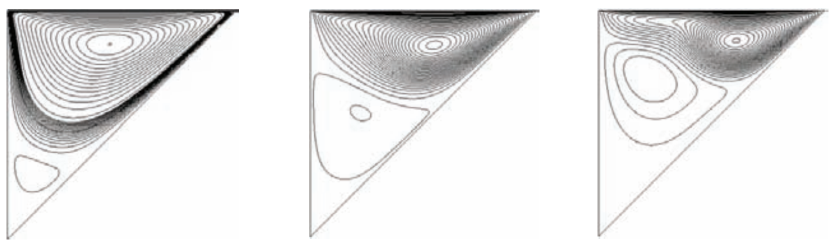

(a) Re=100 (b) Re= 500 (c) Re=1000

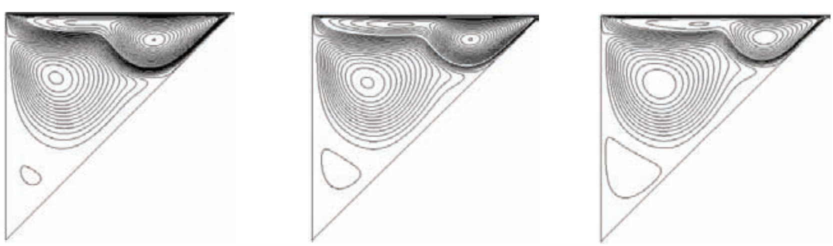

(d) Re=1500 (e) Re=2000 (f) Re= 2500

FIGURE 7 Streamline pattern for isosceles triangular type 'b'

The location of the primary vortex is presented in the next **TABLE 7.**

TABLE 7 Location of the centre of the primary vortex for isosceles triangular cavity type 'b'

Reynolds number	*Reference (Erturk & Gokcol ,2007)*	*Obtained Results by using LBM scheme*
100	*(0.4473,0.8516)*	*(0.4450,0.8500)*
500	*(0.5469,0.8496)*	*(0.5550,0.8500)*
1000	*(0.6094,0.8691)*	*(0.6050,0.8650)*
1500	*(0.6582,0.8848)*	*(0.6567,0.8833)*
2000	*(0.6953,0.8965)*	*(0.6900,0.8933)*
2500	*(0.7227,0.9043)*	*(0.7167,0.9033)*

FIGURE 8 depicts the effect of the Reynolds number to location of the centre of the primary vortex. As indicated in the figure, the primary vortex moved upward to the right as the Reynolds number increases. This behaviour is further validated in TABLE 6 above which present the coordinate of the primary vortex with respect to the Reynolds number.

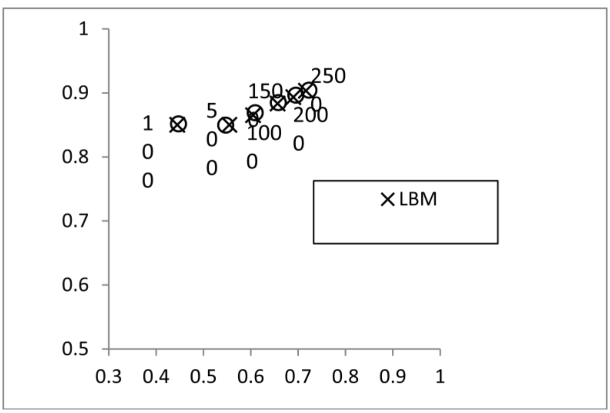

FIGURE 8 Effect of the Reynolds number to the location of the centre of the primary vortex for isosceles triangular type 'b'

3.4 Isosceles triangular type 'c'

The results in term of streamline patterns for isosceles triangular type 'c' is presented in **FIGURE 9** (a) –(f) below.

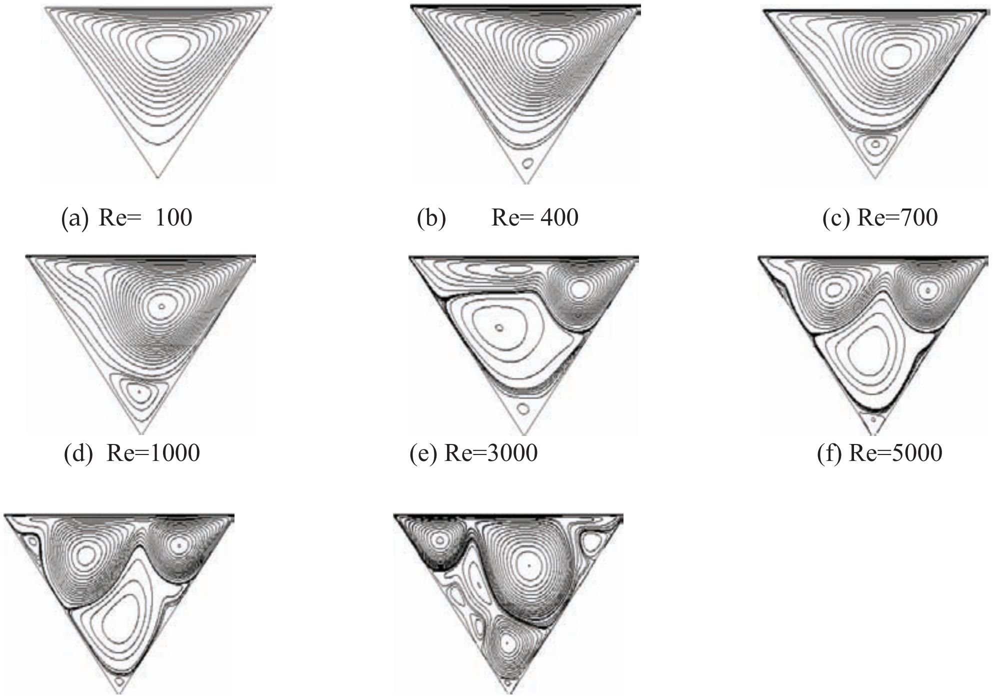

(a) Re= 100 (b) Re= 400 (c) Re=700

(d) Re=1000 (e) Re=3000 (f) Re=5000

(g) Re= 7000 (h) Re=10000

FIGURE 9 Streamline pattern for isosceles triangular type 'c'

In **FIGURE 9** shown above, the flow contours (streamline patterns) with different Reynolds numbers are presented. The flow patterns reveal two significant features. Firstly, as Re numbers are increased, the primary vortex (eddy) moves downstream to the right. For an instance, at Re=100, the location of primary vortex is roughly at 4/5 from the bottom vertex as shown in **FIGURE 9** (a). Apart from the secondary vortex, no other vortex is visible for Re=100. However, for Re=400, there is secondary vortex located near the stagnant corner of the triangle as shown in **FIGURE 9** (b). The shape of this secondary vortex becomes larger as Reynolds numbers is further increased as shown in **FIGURE 9** (d) to **FIGURE 9 (**h).

The second significant feature is the number of vortices in the cavity which is increased as the Re number is increased. **FIGURE 9** (e) shows that the third secondary vortex appears for Re=3000, located about 3/5 from the bottom corner of the cavity. The primary vortex moves further upstream to the left before splitting into another secondary vortex when Re=5000, as shown in **FIGURE 9** (f). For Re=7000 and Re=10000, the numbers of vortex in the cavity are five and six respectively.

TABLE 8 Location of the centre of the primary vortex for isosceles triangular type 'c'

Reynolds number	*Results obtained by LBM*
100	*(0.5450,0.7600)*
400	*(0.6100,0.7500)*
700	*(0.5950,0.7150)*
1000	*(0.5875,0.7150)*
3000	*(0.7400,0.8200)*
5000	*(0.7350,0.8100)*
7000	*(0.7583,0.6200)*
10000	*(0.4117,0.5375)*

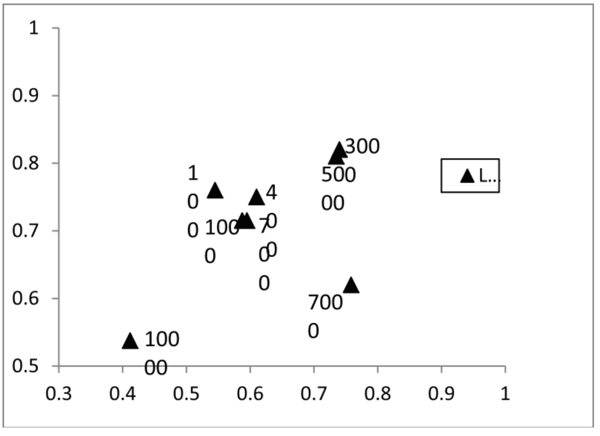

FIGURE 10 Effect of the Reynolds number to location of the centre of the primary vortex for isosceles triangular type 'c'

From the **FIGURE 10** above, initially the primary vortex moves to upstream to the right as Reynolds number increases. However, at Re=3000 onwards, the primary vortex moves downstream to the left. This profile is significantly different that profile for the other two type of triangular cavities shown in previous sections.

4.0 Conclusion

Among the microscopic models existing in the literature, LBM, the model developed from continous Boltzmann equation, has evolved into a powerful tool for modelling complex flow since it was first appeared in 1980s. Although the approach is based on the microscopic interactions, all macroscopic continuum equations such as the Navier-Stokes equation can be derived and recovered.

Fluid flow behaviours in shear driven cavities have been demonstrated by using Lattice Boltzmann scheme successfully. It was found that, the present approach correctly predicted the flow feature for different Reynolds numbers and yield excellent agreement with the results from previous works. The streamline contours or patterns are in good agreement with Ghia et al., and Erturk et. al.
Apart from that, it is found that the streamline patterns are heavily affected by the Reynolds number and also the geometry of the cavity.

However there are few demerits of LBM. When Reynolds number is large, the relaxation parameter in the LBM approaches to the stability margin if the number of mesh points is not very large. There are few solutions have been proposed (He et al., 1996). However, a novel solution to this problem is still required. There is also not sufficient evidence to show that the LBM can be applied to aerodynamic turbulent flows. At present time, one of the weaknesses of LBM for Computational Fluid Dynamics (CFD) is the lack of turbulence modelling. The application of LBM to turbulent flows at high Reynolds number remains as an area of future development.

5.0 Acknowledgment

The authors would like to acknowledge Universiti Teknikal Malaysia Melaka and Universiti Teknologi Malaysia for supporting this work through research grant.

6.0 References

Albensoeder, S. & Kuhlmann, H.C.(2005).Accurate three-dimensional lid-driven cavity flow. *Journal of Computational Physics*, Vol. 206, 536-558. ISSN 0021-9991

Anderson, D.J.(1995), *Computational Fluid Dynamics*, McGraw-Hill, Singapore.

Bhatnagar, P. L., Gross, E. P. and Krook,M.(1954). A Model for Collision Processes in Gasses. 1. Small Amplitude Processes in Charged and Neutral One Component. *System Physics Review*, Vol. 94, 511–525.

Cheng M. & Hung K.C. (2006).Vortex Structure of Steady Flow in a Rectangular Cavity. *Computers & Fluids*, Vol. 35, n. 1, pp. 1046-1062. ISSN 0045-7930.

Duan, Y.L. & Liu,R.X. (2007). Lattice Boltzmann Simulations of Triangular Cavity Flow and Free-Surface Problems. *Journal of Hydrodynamics,* Vol.19, n.2, pp. 127-134.ISSN 1001-6058.

Erturk E. & Dusun, B. (2007). Numerical Solutions of 2-D Steady Incompressible in a Driven Skewed Cavity. *Journal of Applied Mathematics and Mechanics*. Vol. 87, pp 377-392. ISSN 0021-8928.

Erturk, E. & Gokcol O.(2007). Fine Grid Numerical Solutions of Triangular Cavity Flow. *The European Physical Journal Applied Physics*, Vol.38, pp. 97-105, ISSN 1286-0042.

Erturk E. ; Corke T.C. & Gokcol, O. (2005).Numerical Solutions of 2-D Steady Incompressible Driven Cavity Flow at High Reynolds Number, *International Journal for Numerical Methods in Fluids*, Vol.48, pp. 747-774. ISSN 1097-0363.

Francois, C. (1989). Derivation of Slip Boundary Conditions for the Navier-Stokes System from the Boltzmann Equation. *Journal of Statistical Physics*. Vol. 54. ISSN 1572-9613.

Frish, U. ; Hasslacher, B. & Pomeau, Y.(1986). Lattice Gas Automata for the Navier- Stokes Equation. *Physics Review Letter*. Vol. 56, pp. 1505-1508. ISSN 1079-7114.

Ghia, U. ; Ghia, K.N. & C.Y. Chin, (1982). High Re Solutions for Incompressible Flow Using The Navier-Stokes Equations and a Multigrid Method, *Journal of Computational Physics*, Vol. 48, pp. 387-411. ISSN 0021-9991

Gladrow ,D.G. (2000). *Lattice Gas Cellular Automata and Lattice Boltzmann Models*, A*n Introduction*. Springer. New York.

He, X. & Doolen, G. (1997). Lattice Boltzmann Method on Curvelinear Coordinates System: Flow around a circular cylinder. *Journal of Computational Physics*, Vol 134,pp. 306-315. ISSN 0021-9991

He, X. and Luo, L.S.(1997). Lattice Boltzmann Model for the Incompressible Navier-Stokes Equations. *Journal of Statistical Physics*. Vol. 88, pp. 927-944. ISSN 1572-9613.

Hou, S., Q., Zou, S., Chen and, Doolen, G.(1995). Simulation of Cavity Flow by the lattice Boltzmann Method. *Journal of Computational Physics*. Vol. 118, 329-347. ISSN 0021-9991.

Houat, S. & Youcefi, A. (2011). Two Dimensional Simulation of Incompressible Fluid Flow Using Lattice Boltzmann Method, *International Review of Mechanical Engineering*, Vol .1,n. 3, pp. 286 – 292. ISSN 1970-8734.

Kampen, V.N. G. (1987). Chapman-Enskog as an Application of the Method for Eliminating Fast Variables. *Journal of Statistical Physics*. Vol. 46, Nos. ¾. ISSN 1572-9613.

Liboff, R.L.(1990). *Kinetic Theory.* Prentice-Hall, Englewood Cliff New Jersey.

Malapinas, O. ; Fieter, N. & M. Deville, Lattice Boltzmann Method For The Simulation of Viscoelastic Fluid Flows, *Journal of Non-Newtonian Fluid Mechanics*, Vol. 165, pp. 1637-1653, 2010. ISSN 0377-0257.

Mohd Irwan, M.A. ; Fudhail, A. M. ; Nor Azwadi, C. S. & Masoud, G. (2010). Numerical Investigation of Incompressible Fluid Flow through Porous Media in a Lid Driven Square Cavity, *American Journal of Applied Sciences*, Vol. 7, n. 10, pp. 1341-1344.ISSN 1554-3641.

Munir, F.A. ; Sidik,N.A.C . & Ibrahim,N.I.N.(2011). Numerical Simulation of Natural Convection in An Inclined Square Cavity, *Journal of Applied Sciences,* Vol. 11, n2, pp.373-378. ISSN 1812-5654.

Reider, M.B. & Sterling, J.D. (1995). Accuracy of discrete velocity BGK models for the simulation of the incompressible Navier-Stokes equation. *Computer and Fluids,*Vol 24, pp. 459-467. ISSN 0045-7930.

Sidik, N.A.C, The Development of New Thermal Lattice Boltzmann Models for The Simulation of Thermal Fluid Flow Problems. Ph.D. dissertation, Faculty of Science & Technology, Keo Univ., Japan, 2007.

Sterling, J.D. (1996). Stability Analysis of Lattice Boltzmann Methods. *Journal of Computational Physics,* Vol 123,n.1,pp. 196-206. ISSN 0021-9991.

Succi, S.(2001). *The Lattice Boltzmann Equation for fluid dynamics and beyond*. Oxford Science Publications, New York.

Sukop, M.C. and Thorne, D.T. (2006). *Lattice Boltzmann Modeling : An introduction for geoscientists and engineers*. Springer, New York.